Palladium Phosphide Nanoparticles as Highly Selective Catalysts for the Selective Hydrogenation of Acetylene

Yanan Liu,[1,2] Alan J. McCue,[3] Chenglin Miao,[1] Junting Feng,[1]* Dianqing Li[1] and James A. Anderson[2]*

[1] State Key Laboratory of Chemical Engineering, Beijing University of Chemical Technology, Beijing 100029, China.

[2] Surface Chemistry and Catalysis Group, Materials and Chemical Engineering, Department of Engineering, University of Aberdeen, Aberdeen, UK, AB24 3UE.

[3] Department of Chemistry, University of Aberdeen, Aberdeen, UK, AB24 3UE.

Tel: +44 1224 272838, Email: lidq@mail.buct.edu.cn; j.anderson@abdn.ac.uk

Abstract

Pd_3P and PdP_2 phases of *ca*. 4 nm were prepared on a TiO_2 support by an impregnation route. Data from the hydrogenation of acetylene under both non-competitive and competitive conditions showed that PdP_2/TiO_2 exhibits enhanced selectivity and stability relative to Pd_3P. Furthermore, the selectivity produced over PdP_2 (84% ethylene selectivity @ 100% acetylene conversion) compares favorably with recently reported materials. XPS and CO-IR measurements reveal that the incorporation of P helps to break up contiguous Pd sites. This in turn is thought to affect the adsorption and desorption of reactants/products and thus improves selectivity. This work reveals that the incorporation of P into Pd materials could be regarded as a promising approach to develop new and improved Pd-based catalyst by creating a means to control the nature of the active sites.

Keywords

Palladium phosphide, selective hydrogenation, alkyne, acetylene, ethylene, site-isolation

Introduction

Ethylene is a key intermediate and product in the petrochemical industry with the majority being used for polyethylene production. Traditionally, it has been produced from steam

cracking of naphtha [1,2,3,4]. However, the emergence of a plentiful supply of low cost ethane from shale gas means that steam cracking of ethane is growing in popularity [5,6]. Both approaches tend to produce undesired unsaturated hydrocarbons which can poison polymerization catalysts unless removed down to low ppm levels. For example, naphtha cracking yields 0.5-2% of acetylene [1,4]. The preferred method for reducing acetylene to an acceptable level is selective hydrogenation since this yields additional ethylene and therefore maximizes the profitability.

Supported Pd catalysts are commonly employed in these processes but exhibit unsatisfactory selectivity and stability unless, for example, alloyed with a second metal [3,4]. Alloying is thought to serve multiple functions. Firstly, it breaks up contiguous Pd sites, which have a greater barrier for desorption of ethylene relative to that of hydrogenation [7,8]. Secondly, alloying limits hydrogen migrating into the bulk of Pd to form palladium hydride with good evidence linking hydride formation to over-hydrogenation [9,10,11,12,13,14]. Industrially, Ag is the most commonly utilized metal for alloying, although a number of alternatives have been reported in the literature [15,16,17,18,19]. In some cases the role of the second metal is merely structural, although in other examples the second metal (i.e., Cu) may pay an active role in the catalytic mechanism [20,21,22,23,24,25]. Even though alloying enhances selectivity, it is not uncommon to co-feed CO as a competitive adsorbate to limited ethylene adsorption at high levels of acetylene conversion [3]. The difficulty with this latter approach is that the amount of CO added must be regulated in real-time to avoid deactivating the catalyst to an extent where 'acetylene slip' occurs [2,3,26].

In recent years a number of alternative approaches to control selectivity have been reported which include using sulfur and phosphorous molecules as selectivity modifiers [27,28,29,30], intermetallic compounds [31,32,33], metal oxides such as CeO_2 [34,35] and In_2O_3 [36] or site-isolated Pd atoms constrained within a C_3N_4 host [37]. All of these examples are similar in that the environment around the active site is both uniform and well-defined. Inspired by success using sulfur compounds to enhance the selectivity of Pd catalysts, recently attention was given to palladium sulfide (specifically the Pd_4S phase) where exceptionally promising results were obtained which were attributed in part to a 'site isolation' effect [38,39,40].

Albani *et al*. subsequently published a molecular level understanding for Pd_3S/C_3N_4 as a catalyst and attributed the stellar performance to site-isolated Pd trimers [41]. In that work, Pd_3S and Pd_4S are compared and shown to be similar, yet subtly different.

Encouraged by the performance of palladium sulfide attention was turned to palladium phosphide materials which have already attracted considerable interest in magnetic [42], electronic [43,44], optics [45,46], energy storage [47,48] and catalytic applications [49,50] but are less well studied than the analogous nickel phosphides [51]. In terms of heterogeneous catalysis, this class of materials offers fascinating properties such as tunable composition (i.e., $Pd_{15}P_2$ to PdP_3 phases known to exist) and controllable crystallinity. For example, several studies have shown that metal phosphides (e.g., NiP [52,53], CoP [54,55] and RhP [56]) are highly active toward hydrodesulfurization (HDS) and hydrodenitrogenation (HDN) of petroleum feedstocks. Moreover, Ni−P nanoparticles have recently been explored for the chemoselective hydrogenation of phenylacetylene [57]. However, there are few reports in the case of palladium phosphide [58], particularly with regards to the selective hydrogenation of acetylene. Herein, the synthesis of two TiO_2 supported palladium phosphides with different Pd/P ratios are described. Detailed characterisation showed that either Pd_3P or PdP_2 phases were formed with selectivity linked to the unique active site arrangement created by incorporation of P.

2. Experimental

2.1. Materials

Chemical reagents including $PdCl_2$ (Johnson Matthey), NaCl (Fisher Scientific), $NH_4H_2PO_2$ (Alfa Aesar) and P25 TiO_2 (Aldrich) were purchased and used without further purification. Deionized water (electrical conductivity < 10^{-6} S cm^{-1}) was used in all the experimental steps.

2.2. Synthesis of TiO_2 supported Pd_xP_y catalysts

Palladium phosphide catalysts with different Pd/P ratios were prepared by an impregnation method [59]. Firstly, Pd/TiO_2 (2 or 10 wt% Pd) was prepared by incipient wetness impregnation using $PdCl_2$ dissolved in 1 mol L^{-1} aqueous HCl. A slurry was formed (2 g of TiO_2) and stirred for 2 h before being dried at 120°C. Next, Pd/TiO_2 was impregnated with phosphorous by adding an aqueous solution of 1 mol L^{-1} $NH_4H_2PO_2$ with stirring for 2 h followed by drying at 70°C, to

give samples with nominal Pd/P molar ratios of 3:1 and 1:2. The materials were then reduced in 20% H_2/N_2 (25- ml min^{-1}) at 500°C for 4 h with a heating rate of 10°C min^{-1}. Samples are denoted as 2 or 10% Pd_xP_Y/TiO_2 where x and y denote the palladium phosphide stoichiometry/phase (either Pd_3P or PdP_2).

2.3. Catalyst characterization

X-ray Diffraction (XRD) patterns were recorded on an X'Pert powder diffractometer (PANalytical) fitted with a PIXcel1D detector using Cu Kα radiation (λ = 0.154 nm) at 2θ = 20-85º with a step size of 0.013°. The phase compositions were determined by Rietveld refinement using HighScore Plus software [60]. The particle size and structure of samples were determined using a JEOL JEM-2100F high-resolution transmission electron microscope (HRTEM) combined with energy dispersive X-ray spectroscopy (EDX) to examine composition. Elemental analysis for Pd was performed using a Shimadzu ICPS-7500 inductively coupled plasma atomic emission spectrometer (ICP-AES). Temperature-programmed reduction and oxidation experiments (TPR and TPO, respectively) were performed on a TPDRO 1100 instrument with a thermal conductivity detector (TCD). The sample (100 mg) was loaded in the bottom of quartz reactor. TPR profiles were collected in a temperature range of 30-250°C using a heating rate of 5°C min^{-1} and 5% H_2/N_2 as the reductant gas (20 ml min^{-1}). The hydrogen consumption was quantified based on a response factor determined using a high purity CuO standard. Carbon deposition was analyzed by conducting TPO-MS experiments. Used catalyst samples were heated in 5% O_2/N_2 (20 ml min^{-1}) from room temperature to 600°C with a heating rate of 10°C min^{-1}. In situ diffuse reflectance Fourier Transform Infrared (DRIFT) spectroscopy of adsorbed CO was obtained with a Bruker Tensor 27 instrument with a resolution of 4 cm^{-1}. Samples were first treated at 250°C in N_2 for 30 min, before being cooled to room temperature and evacuated to *ca*. 10^{-4} mbar before a background was recorded. Then the samples were exposed to a 99.9% CO flow for another 30 min. A spectrum was then obtained after further evacuation to *ca*. 10^{-4} mbar. X-ray photoelectron spectra (XPS) of samples were measured to obtain the surface atomic ratios from a Shimadzu AXIS Supra X-Ray Photoelectron spectrometer equipped with an Al Kα anode. The C1s peak at 284.6 eV was used as the reference.

2.4. Selective hydrogenation of acetylene

Gas phase hydrogenation reactions under non-competitive and competitive conditions were conducted in a Microactivity Reference fixed-bed microreactor (9 mm diameter) at 1 bar pressure using catalyst (50 mg) diluted with SiC (200 mg, 200-450 mesh, Aldrich). Non-competitive reactions were carried out in a flow of 1.2% acetylene/balance N_2 with 2 equivalents of H_2 co-fed relative to acetylene. The competitive tests were performed in a mixture of 0.6% acetylene/5.4% ethylene/balance N_2 with 2 equivalents of H_2 co-fed relative to acetylene. The reactor temperature was varied from 50 to 225°C in 25°C increments with 5 h time on stream (TOS) at each temperature in order access catalyst stability. Prior to reaction, samples were re-reduced in 10% H_2/N_2 at 250°C for 2 h (60 ml min^{-1}). The product distributions were determined by gas chromatography (PE Clarus 580) with a flame ionization detector using an elite alumina capillary column. Conversion is defined as the amount of acetylene reacted divided by the amount introduced. Products selectivity is defined as the amount formed (i.e., ethylene $_{out}$ – ethylene $_{in}$) divided by the amount of acetylene reacted. Negative selectivity indicates that a fraction of the ethylene in the feed is over-hydrogenated to ethane. Selectivity to oligomers was calculated from a carbon balance (100±2%) assuming that the sum of alkene, alkane and oligomers selectivity equaled 100% [22,23].

3. Results and discussions

3.1. Catalytic performance under competitive and non-competitive conditions

The catalytic performance of the 2% loaded samples were first evaluated using experiments with acetylene as the sole hydrocarbon in the feed gas (Figure 1). At 50°C, the P:Pd ratio appeared to have an impact on the initial activity with the Pd_3P phase being more active than PdP_2. Analysis of the absolute Pd loading by ICP (Table S1) suggested that this effect was more likely associated with the nature of the phosphorous phase as opposed to the amount of Pd present in the samples. In terms of selectivity at 50°C, the most active sample, 2% Pd_3P/TiO_2, produced ethylene and ethane in similar amounts (*ca*. 40%) whereas 2% PdP_2/TiO_2 exhibits higher selectivity to ethylene (55%) with oligomers (35%) and ethane (20%) as minor products. The product distribution over PdP_2/TiO_2 may imply that under these conditions

hydrogenation is less prominent or that acetylene coverage is high which promotes coupling reactions to form oligomers. At all temperatures in excess of 50°C, full acetylene conversion was observed. This was deemed beneficial as it meant selectivity could be evaluated under challenging conditions where ethylene adsorption is not impeded by the presence of adsorbed acetylene. Selectivity in the mid temperature range (75-125°C) shows that 2% Pd_3P/TiO_2 favors ethane (40-50%) whereas 2% PdP_2/TiO_2 favors ethylene (55-60%). Increasing temperature further sees a shift in product distribution for both samples towards ethylene. Over 2% Pd_3P/TiO_2, a maximum ethylene selectivity of 78% (Figure 1A) was achieved. PdP_2/TiO_2 shows an exceptional ethylene selectivity of *ca*. 85% (Figure 1B). It could be considered unusual to see alkene selectivity increases as temperature increases, however a number a studies using different catalytic materials have reported similar trends in recent years [34,36,38,39].

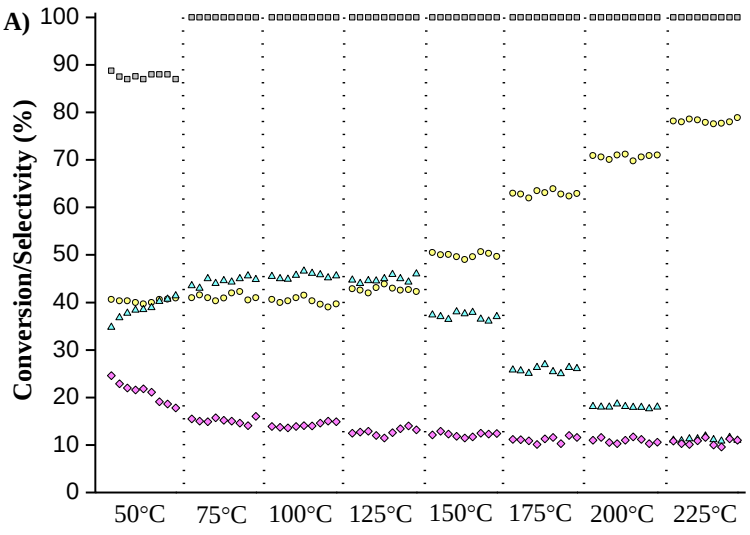

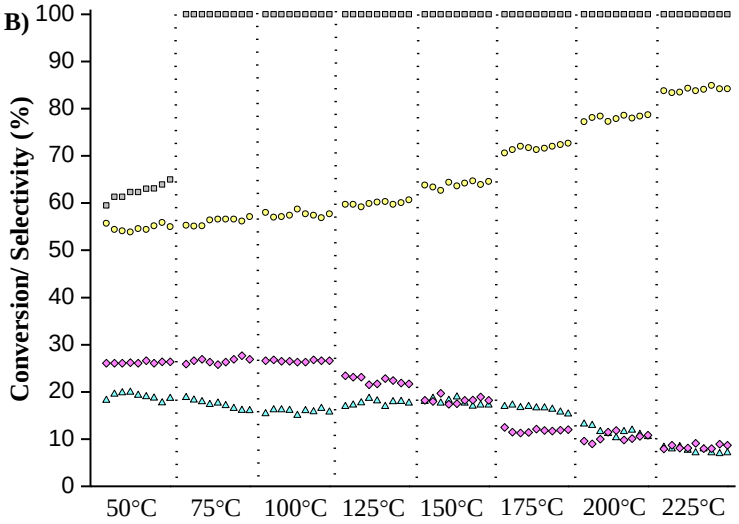

Figure 1. Acetylene conversion (grey squares), ethylene selectivity (yellow circles), ethane selectivity (cyan triangles) and oligomer selectivity (pink diamonds) versus temperature over A) 2% Pd_3P/TiO_2 and B) 2% PdP_2/TiO_2 (acetylene, GHSV: 256000 h^{-1}, H_2: C_2H_2 = 2, 5 h TOS at each temperature).

Tests were then extended to consider the competitive conditions encountered industrially (i.e., acetylene and ethylene both present in the gas feed). Once again, 2% PdP_2/TiO_2 was less active with incomplete acetylene conversion observed at 50 and 75°C (Figure 2). In terms of selectivity at low temperature, Pd_3P and PdP_2/TiO_2 both favored ethylene as a major product once 100% was achieved. At higher temperatures, the product distribution again shifts towards ethylene which is consistent with results for non-competitive tests (Figure 1). At 225°C, ethylene selectivity for 2% Pd_3P and PdP_2/TiO_2, were 70 and 84%, respectively. The maximum ethylene selectivity over PdP_2/TiO_2 fairs well when compared with Pd_4S supported on carbon nanofibers (82% ethylene selectivity) which represents a benchmark for tests conducted under equivalent conditions [38].

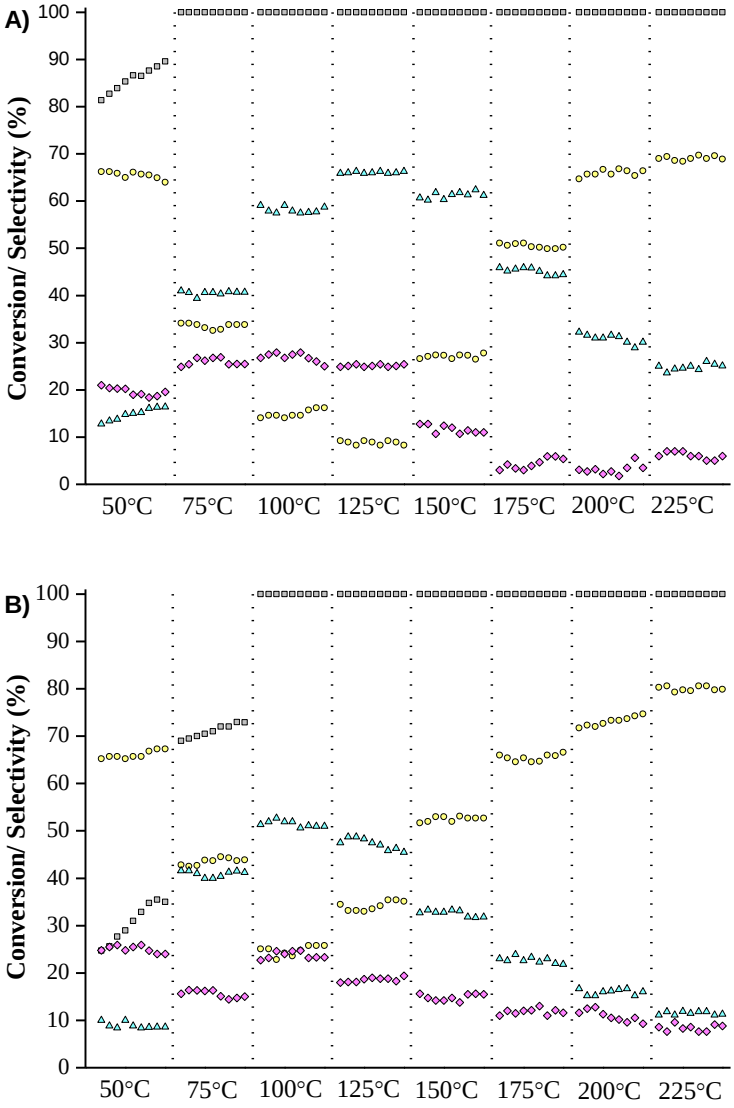

Figure 2. Acetylene conversion (grey squares), ethylene selectivity (yellow circles), ethane selectivity (cyan triangles) and oligomer selectivity (pink diamonds) versus temperature over A) 2% Pd_3P/TiO_2 and B) 2% PdP_2/TiO_2 (mixed acetylene/ethylene, GHSV: 256000 h^{-1}, H_2: C_2H_2 = 2, 5 h TOS at each temperature).

The apparent activation energy (Ea) is a valuable parameter to judge catalyst performance and can be determined from a plot of the natural logarithm of turnover frequency (ln TOF) *versus* 1000/T using data obtained under low conversion [61,62]. Of course, data is only of value if collected under conditions which are not subject to mass or heat transfer limitations. To ensure this was the case, Weisz-Prater and Mears criterion calculations [63,64,65] were performed (see supporting information). Following this approach, apparent activation energies of 39.5 and 34.9 kJ mol^{-1} were determined for 2% PdP_3/TiO_2 and PdP_2/TiO_2 catalysts,

respectively. Whilst the difference is relatively small, it is interesting to note, especially as the PdP_2 sample is more active (Figures 1 and 2).

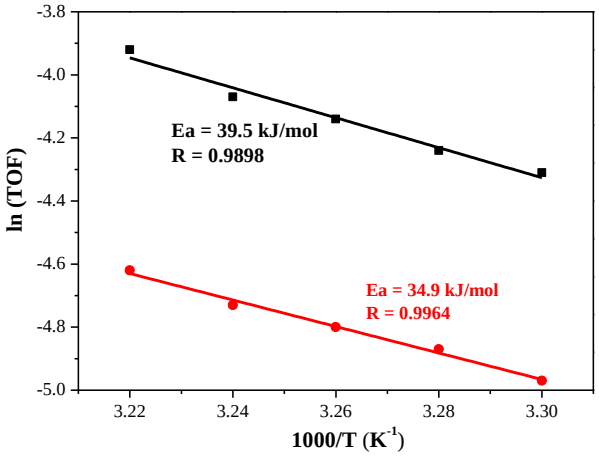

Figure 3. Plots of the natural logarithm of TOF versus 1/T (30-38°C) over 2% Pd_3P/TiO_2 (black) and 2% PdP_2/TiO_2 (red) showing the apparent activation energy at low conversion.

3.2. Catalyst stability

The performance of 2% Pd_3P and PdP_2/TiO_2 catalysts under both competitive and non-competitive conditions is promising. However, one of the biggest challenges for acetylene hydrogenation catalysts is stability as acetylene derived-oligomers gradually deposit coke on the catalyst leading to the need to regenerate [4]. It is inherently difficult to access both selectivity and deactivation from a single test. This is because deactivation should be accessed under conditions of incomplete conversion where higher selectivity is easier to achieve. It has also been reported that the amount of oligomers formed increases at or near complete conversion [38]. It was decided to assess the stability of ethylene selectivity at complete conversion over a 50 h period (Figure 4). Importantly, it should be noted that the space velocity used in this work is around 50 fold higher than typically used in industry. This means that over an equivalent period of time, the phosphide catalysts are exposed to a substantial amount of acetylene. When assessed on this basis, 2% Pd_3P/TiO_2 showed a 10% decrease in ethylene selectivity over 50 h TOS. In contrast, 2% PdP_2/TiO_2 showed remarkable stability, maintaining a selectivity of *ca*. 82% throughout the same time period. In order to access carbon deposition, used catalysts were studied by TPO-MS. A mass loss of 1.56 wt% C was removed from 2% Pd_3P/TiO_2 which had been subjected to 50 h TOS, considerably greater than the 1.07 wt% C lost from 2% PdP_2/TiO_2. The enhanced resistance to coke deposition explains why the PdP_2 catalyst is the more stable of the two (Figure 4).

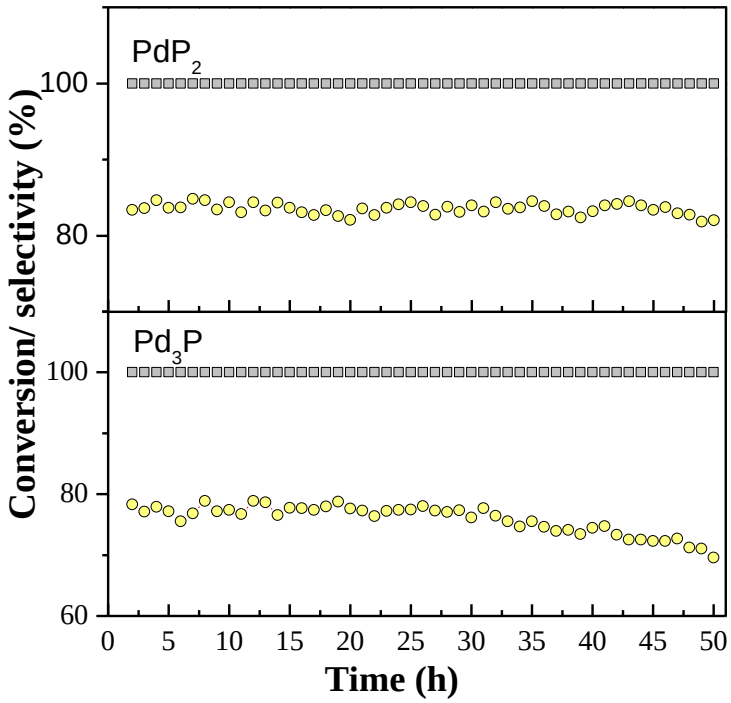

Figure 4. Acetylene conversion (grey squares) and ethylene selectivity (yellow circles) at 225°C A) 2% Pd_3P/TiO_2 and B) 2% PdP_2/TiO_2 (mixed acetylene/ethylene, GHSV: 256000 h^{-1}, H_2: C_2H_2 = 2).

3.3. Phase composition, particle size and uniformity of TiO_2 supported Pd_XP_Y catalysts

To investigate the phase properties of the palladium phosphide samples, powder XRD patterns were collected. However, due to the small particle size (see TEM discussed later) and low metal loading, the patterns did not yield useful information. It therefore proved necessary to prepare analogous samples with a higher metal loading (10 wt%) to aid attempts at characterisation. Attempts to create links between samples of different loadings can be justified if both the high and low loaded samples exhibit similar catalytic behavior. In order to evaluate this, tests were conducted under both non-competitive (Figure S1, activity trend: PdP_2 < Pd_3P, selectivity trend: Pd_3P < PdP_2) and competitive conditions (Figure S2) with results indicating that similar performance trends were obtained regardless of loading. Therefore, XRD patterns of the 10 wt% loading are presented in Figure 5. The patterns are largely dominated by peaks associated with the P25 support (anatase and rutile mixture). Beyond these, features are present in positions which match those expected for Pd_3P (PDF 01-089-3046) and PdP_2 (PDF 00-077-1421). The patterns were analyzed further using Rietveld

refinement to determine the phase composition using structural models of phosphides [66,67] which resulted in small reliability factors implying an appropriate fit (Table 1). Based on this analysis, 10% Pd_3P/TiO_2 would appear to contain predominantly Pd_3P with minor contributions from $Pd_{4.8}P$ impurities. Similarly, 10% PdP_2/TiO_2 was a largely pure phase with < 2% of the palladium phosphide present as PdP_3.

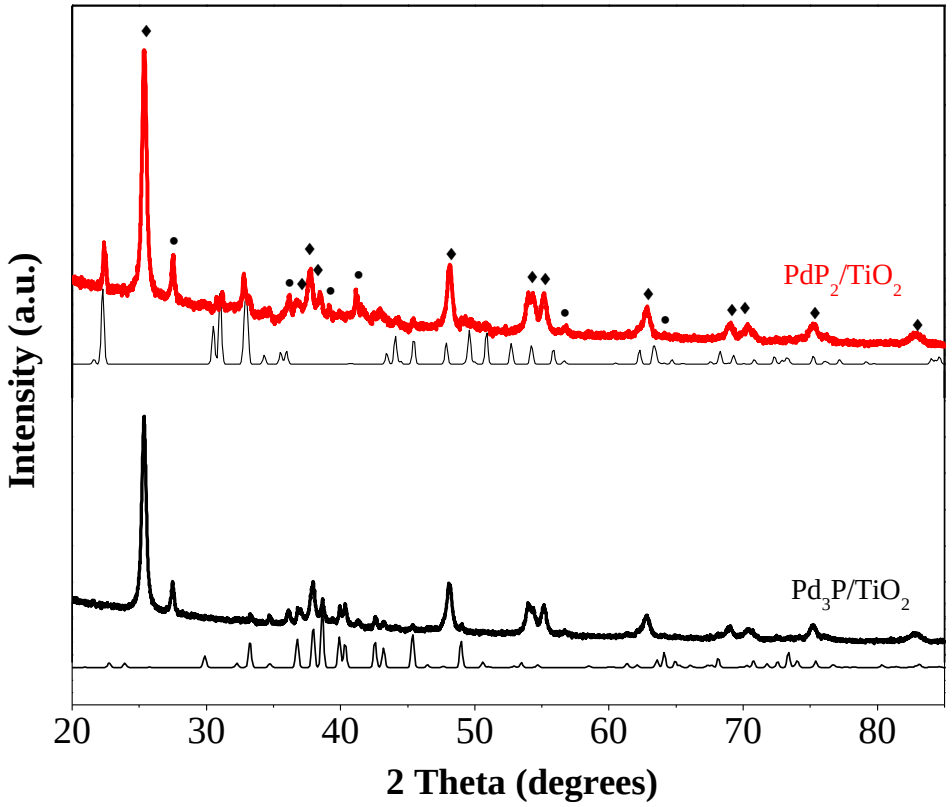

Figure 5. XRD patterns of 10% Pd_3P/TiO_2 (lower, black) and 10% PdP_2/TiO_2 (upper, red). Reference patterns for Pd_3P and PdP_2 are shown below the corresponding sample. Peaks associated with the support are denoted as: ♦ anatase, ● rutile.

Table 1. Phase composition of supported palladium phosphide samples determined by XRD refinement based on structural models of the phosphide phases.

Sample	XRD phase composition of Pd_xP_y		XRD composition of Pd_xP_y		Weighted R Profile
			Pd (wt.%)	P (wt.%)	
10% Pd_3P/TiO_2	Pd_3P (97.6)	$Pd_{4.8}P$ (2.4)	91.1	8.9	1.6985
10% PdP_2/TiO_2	PdP_2 (98.4)	PdP_3 (1.6)	63.0	37.0	2.1045

HRTEM was performed on both 2 and 10 wt% palladium phosphide samples to further confirm similarities in composition despite variation in loading. Representative images of the low weight loadings samples are shown in Figure 6 along with particle size distributions determined from *ca*. 100 particles. 2% PdP_2/TiO_2 sample had a smaller particle size of 3.6 ± 0.4 nm (Figure 6B), although this was only slightly smaller than 2% PdP_3/TiO_2 which was 4.3 ± 0.6 nm (Figure 6A). Importantly, at high magnification, lattice fringes were observed for the 2 wt% loaded samples (Figures 6, A3 and B3) which matched the phase assignment from XRD for the 10 wt% samples. This suggests that sample preparation yields the same primary phase regardless of Pd metal loading (i.e., the synthetic method is both flexible and reproducible). In particular, lattice fringes of 0.223 and 0.271 nm were noted which are close to those expected for pure crystalline Pd_3P (031) and PdP_2 (211) spacings. It should also be noted that these same lattice fringes were observed for the equivalent 10 wt% loaded samples (Figure S3).

Table 2 Composition of TiO_2 supported palladium phosphide samples determined by EDX and XPS.

Samples	EDX composition of Pd_XP_Y		EDX bulk	XPS surface
	Pd (wt.%)	P (wt.%)	Pd:P ratio	Pd:P ratio
10% Pd_3P/TiO_2	88.6	11.4	2.27	2.52
2% Pd_3P/TiO_2	87.7	12.3	2.08	2.29
10% PdP_2/TiO_2	61.3	38.7	0.46	0.45
2% PdP_2/TiO_2	60.5	39.5	0.45	0.39

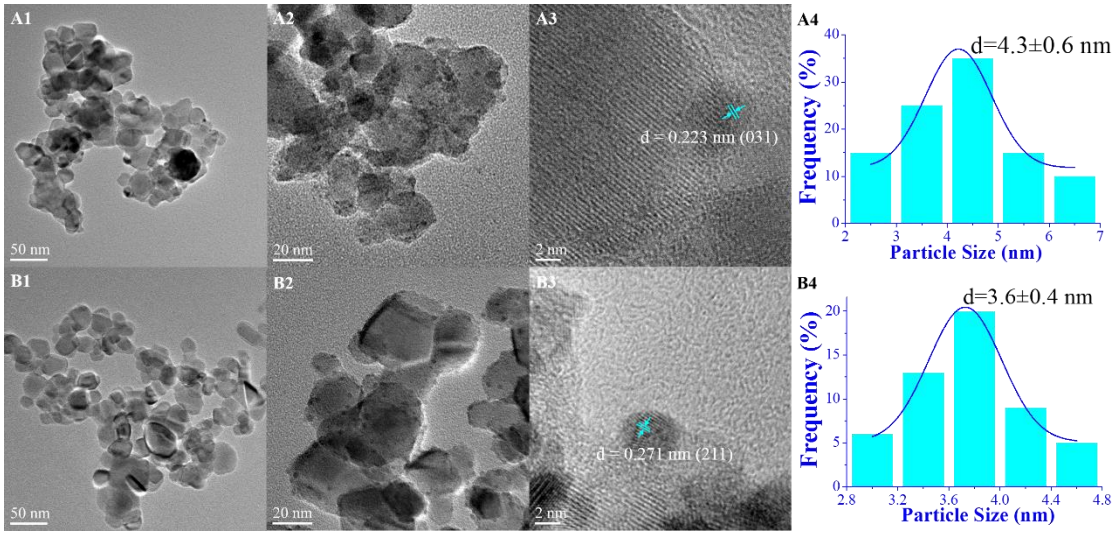

Figure 6. HRTEM images of A) 2% Pd_3P/TiO_2 and B) 2% PdP_2/TiO_2 catalysts. The insets in the corresponding images show the particle size distribution.

The composition of the palladium phosphide component assessed by EDX coupled to HRTEM is presented in Table 2. Note that the EDX analysis from various sample spots yielded equivalent results which suggests the samples are relatively uniform. Comparison of the 10 wt% samples shows that the relative amount of P increases from Pd_3P to PdP_2 as expected. However, the bulk Pd:P ratio for 10% Pd_3P/TiO_2 (2.27) differs considerably from the expected stoichiometry of 3. For 10% PdP_2/TiO_2 sample, the Pd:P ratio of 0.46 is much closer to the expected ratio of 0.50. Similar remarks can be made for the 2 wt% series with 2% Pd_3P/TiO_2 deviating even further (2.08) from the expected stoichiometry. Once again, the 2% PdP_2/TiO_2 sample has a ratio closer to expectation (0.45 vs 0.50). Two key points can be extracted from the results presented in Table 2. Firstly, the weight loading seems to have a fairly small effect on the sample composition, consistent with the similarities in catalytic performance presented earlier. Secondly, the bulk phase palladium phosphide composition always appears to be Pd rich relative to expectation (Table 2). This may be related to the preparation procedure. Initially, a Pd/TiO_2 sample was prepared by incipient impregnation before P was added in a second step. In order to convert the Pd particle into the corresponding Pd_xP_y phase, P must penetrate into the bulk. Although P possesses a smaller atomic radii than Pd, this is unlikely to be a facile process. It is therefore not surprising that such a process occurs readily only at elevated temperatures (500°C in this case) but a 4 h reaction time is insufficient to allow complete transformation. If this hypothesis were correct then it would be expected that the

near surface composition should be richer in P (i.e., since P has to enter and pass through the near surface region to migrate to the bulk). In order to confirm this hypothesis, XPS measurements were conducted. The surface Pd:P ratios determined from XPS are shown in Table 2 and will be described in greater detail later. However, the, results are generally in agreement with the hypothesis as the Pd:P surface ratio is generally higher than the equivalent bulk ratio determined by EDX (Table 2).

3.4 Effect of phosphorous on palladium hydride formation/decomposition

A direct correlation between formation of the β-palladium hydride phase and over-hydrogenation of alkynes is often made [10,68]. Therefore to study hydride formation on Pd_XP_Y samples (via detection of hydride decomposition), TPR profiles were collected and are presented in Figure 6. Both 2% Pd_3P and PdP_2/TiO_2 samples appear to form a hydride phase with decomposition observed as deduced by a negative peak around 70°C [69,70]. Whilst the decomposition temperature is equivalent for both samples, the amount of hydrogen released is not. The H:Pd ratio calculated for 2% Pd_3P/TiO_2 is 0.07 (13.16 µmol H_2/g) , whereas the value for 2% PdP_2/TiO_2 sample is 0.04 (7.35 µmol H_2/g). To place these values into context, a comparison must be made with literature, ideally comparing samples with a similar particle size since dispersion and hydride formation are inherently linked [71]. A monometallic 1% Pd/TiO_2 catalyst (3.5 nm) gave a H:Pd ratio of 0.25 [27]. This indicates that addition of P to Pd particle hinders hydride formation and this may be, in part, relate to enhanced ethylene selectivity. The differences between the two phosphide samples may also go some way to explaining the difference in selectivity at low temperature since Pd_3P/TiO_2 forms a hydride phase to a greater extent and also forms more ethane (Figure 1).

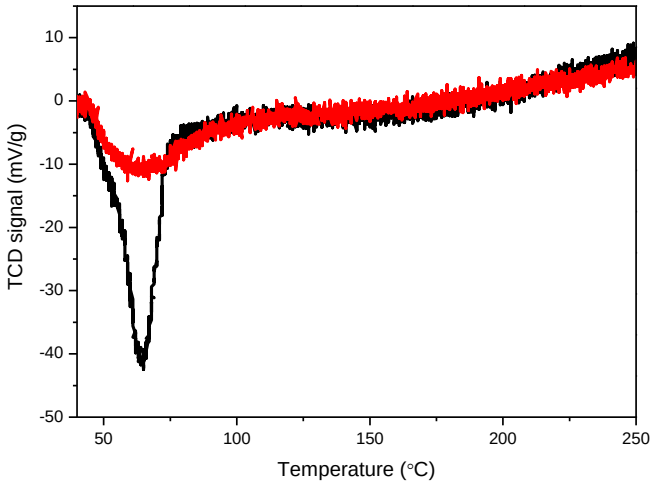

Figure 6. TPR of 2% Pd_3P/TiO_2 (black) and 2% PdP_2/TiO_2 (red).

3.5 Electronic effects and surface structure of TiO_2 supported Pd_XP_Y catalysts

Aspects of the electronic properties of palladium phosphide samples may be inferred from XPS. The P 2p XP spectrum (Figure 8-A) for the 2 wt% loaded samples show a single peak which can be deconvoluted to show contributions due to P $2p_{3/2}$ and $2p_{1/2}$. The position of the peaks (129-131 eV) is far too low to be associated with a phosphate species (i.e., P^{5+}) which has been reported to show a binding energy of around 134 eV for Pd-P materials prepared at low temperature [72,73]. Instead, the peak positon is in broad agreement with the value reported for P in a reduced state (red phosphorous - 130.4 eV) [74]. For 2% Pd_3P/TiO_2 and PdP_2/TiO_2 samples, the maxima associated with the $2p_{3/2}$ peak sits at 129.7 and 130.0 eV, respectively. From this, it is inferred that electron transfer from Pd to P to create a $P^{\delta-}$ species is plausible.

The Pd 3d core level spectrum (Figure 8-B) appears more complex with deconvolution identifying 4 peaks. The peaks centered at 335.0 and 340.5 eV are attributed to the $3d_{5/2}$ and $3d_{3/2}$ signals of Pd, respectively with a neutral charge [75]. The peaks centered at 337.1 and 343.2 eV are assigned to the $Pd_{5/2}$ and $Pd_{3/2}$ signals of Pd^{2+}. It should be noted that the intensity associated with Pd^0 is significantly greater than of Pd^{2+} and that similar spectra have been reported for palladium phosphide materials [72,73]. The oxidized state may occur as a result of Pd oxidation in the absence of a reducing environment, or may correlate with electron donation from Pd to P as suggested from the P 2p XP spectrum. Equivalent comments can

be made concerning the 10% loaded samples (See Figure S4 and S5)

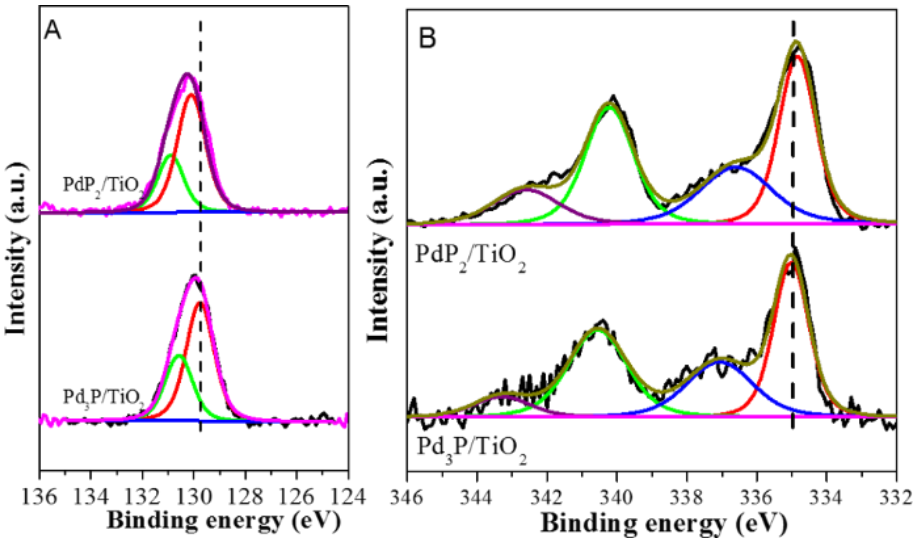

Figure 8. XP spectra of 2% Pd_xP_y/TiO_2 samples. A) The P 2p region. B) The Pd 3d region.

In order to gain insight into the geometric arrangement of Pd atoms on the surface, FTIR spectra of adsorbed CO were collected and are presented in Figure 9. For Pd_3P containing sample, two clear bands are observed at *ca*. 2036 and 1929 cm^{-1}, which are attributed to linear and bridge-bound CO, respectively. In addition, there is a significant amount of tailing on the 1929 cm^{-1} peak towards lower wavenumber which is assigned to three-fold hollow bound CO. This spectrum would therefore indicate a complex mixture of Pd surface sites, including some which are contiguous. The spectrum of the PdP_2 sample shows little intensity beyond 1870 cm^{-1} which may suggest a lower population of three-fold hollow sites. Furthermore, the intensity of the band associated with linearly bound CO increases. Overall, these results suggest that the greater presence of P in PdP_2 compared with Pd_3P acts to break up Pd ensembles.

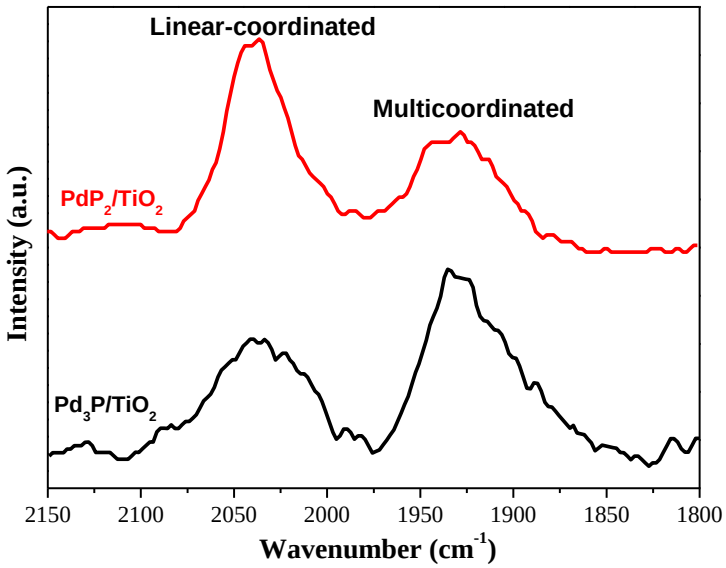

Figure 9. *In situ* FTIR spectra of palladium phosphide catalysts exposed to CO. 2% Pd_3P/TiO_2 (lower, black) and 2% PdP_2/TiO_2 (upper, red).

From XRD (Figure 5 & Table 1) and HRTEM-EDX (Figure 6 & Table 2) analysis it is quite clear which predominant phase exists for each sample. Comparison of these results with XPS data (Figure 7 & Table 2) suggests that the near surface region of Pd_3P and PdP_2/TiO_2 samples have a stoichiometry even closer to that expected from the phase assignment. From the FTIR spectra of adsorbed CO (Figure 9) is clear that the nature of the surface sites differ for both samples. Therefore, in order to try rationalize catalytic performance the crystal structures of PdP_3 and PdP_2 are now considered (note: the following discussion excludes any possible surface relaxation since the necessary calculations fall out with the scope of this work). Since the unit cell of Pd_3P is orthorhombic (a = 5.947, b = 7.451 and c = 5.170 Å) surface models of the (100), (010) and (001) terminations constructed from the crystal structure reported by Rundqvist and Gullman [66] are shown in Figure 10. All three terminations present subtly different arrangements of Pd atoms (which are assumed to be the active sites). The Pd_3P (001) surface exposes both Pd and P atoms with the closest neighbor to Pd being a P atom at a distance of 2.34 Å. On this surface, a Pd-Pd interatomic distance of 2.78 Å exists which is only marginally longer than for elemental Pd (2.75 Å) [76]. For the Pd_3P (100) surface, more extended clusters of Pd atoms are evident. The Pd_3P (010) surface structure is potentially interesting since the shortest possible Pd-Pd interatomic distance (2.93 Å) is considerably

longer than that of monometallic Pd or $InPd_2$ (2.82 Å) and $GaPd_2$ (2.85 Å) intermetallic compounds with enhanced selectivity in the later cases attributed to Pd site isolation due to elongated Pd-Pd distances [77]. It therefore seems plausible that the Pd atoms on the Pd_3P (010) surface may act as isolated sites (Figure 10). If that were the case, it would be desirable to prepare a sample where the (010) surface is preferentially exposed. However, in this work, no control of the surface termination was attempted. It seems reasonable to assume, based on the analysis above, that a combination of the different sites must exist (red blocks, Figure 10) with the problem being, that contiguous Pd sites are likely to be less selective [10]. This assessment about the presence of contiguous sites being derived from FTIR of adsorbed CO (Figure 9). Specifically, sites for 3-fold hollow bound CO exist – contiguous sites on the (100) surface or in the depressions between the 1st and 2nd Pd layer on the (010) and (001) surfaces.

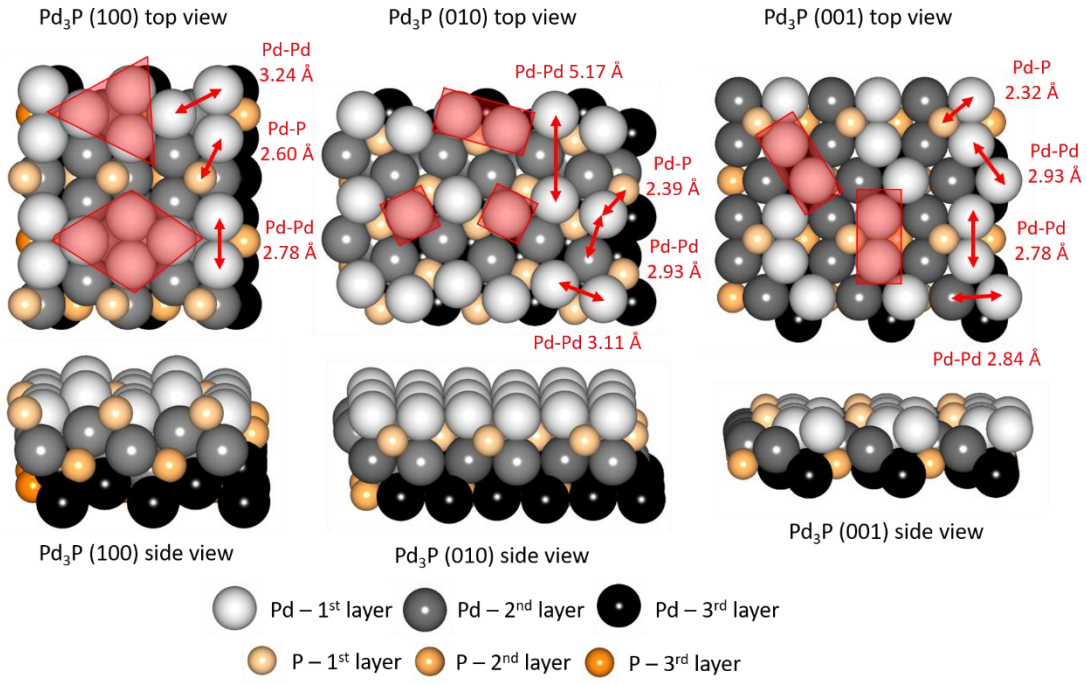

Figure 10. Structures of Pd_3P (100), (010) and (001) surfaces based on the crystal structure reported by Rundqvist and Gullman [66]. Arrows and dimensions correspond to interatomic distances. Red blocks indicate shapes of accessible surface Pd sites.

Equivalent surface models for the (100), (010) and (001) PdP_2 surfaces, based on the monoclinic crystal structure (a = 6.207, b = 5.858 and c = 5.874 Å) reported by Zachariasen,

are shown in Figure 11 [67]. Regardless of the surface termination, it is clear that Pd atoms are more uniformly separated or isolated and this is likely to contribute to the enhanced selectivity of PdP_2 relative to the Pd_3P phase. The PdP_2 (010) and (001) surfaces appear to present chains of Pd atoms, although the interatomic distances are 3.10 Å which means these are more likely to act as isolated sites, perhaps with the next nearest P atom playing a role (Pd-P separation 2.34 Å) which would be similar to Pd_3S [41] and CeO_2 [34] where a non-metal atom participates in the proposed mechanism. The most striking example of site isolation comes from the PdP_2 (100) surface where the Pd atoms are 4.15 Å apart. It would be highly desirable to prepare samples which preferentially expose this surface, whether via epitaxial growth, or shaped controlled nanoparticle synthesis. These remarks are largely in agreement with characterisation data presented, although FTIR of adsorbed CO still suggests a bridged bound species exists, albeit of relatively low intensity. It seems possible that CO can bridge atoms at the elongated Pd-Pd distance, or that alternative (higher index) surface terminations may exist with different atoms arrangements, not considered above. Lastly and with regards to oligomer formation, it seems reasonable to assume that oligomerisation requires the coupling of two molecules occupying adjacent sites. Based on the discussion above, it would be expected that this would occur more readily on the Pd_3P catalyst and which is consistent with results of the longer term stability tests and TPO measurements (Figure 4).

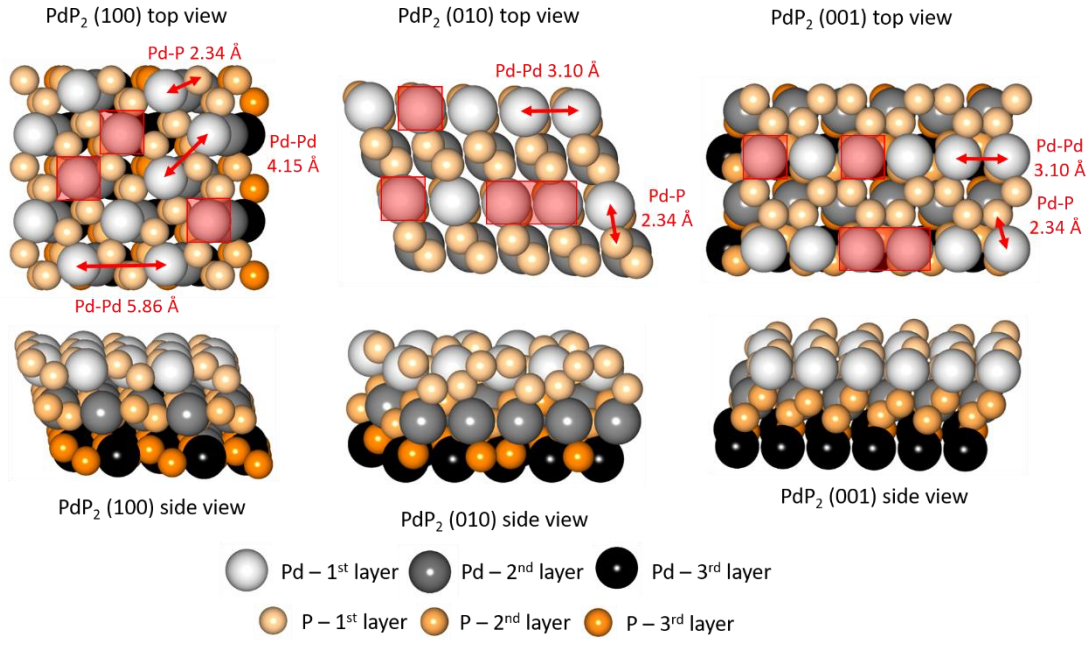

Figure 10. Structures of PdP_2 (100), (010) and (001) surfaces based on the crystal structure reported by Zachariasen [67]. Arrows and dimensions correspond to interatomic distances. Red blocks indicate shapes of accessible surface Pd sites.

Conclusions

TiO_2 supported Pd_3P and PdP_2 phases were prepared with *ca*. 4 nm particle size from a simple impregnation method. Characterisation by XRD, TEM and XPS confirmed these specific phases were formed in high purity. Acetylene hydrogenation tests indicated that both catalysts exhibited excellent ethylene selectivity, although samples with the PdP_2 phase present were inherently more selective. Characterisation of adsorbed CO by FTIR indicated P acted to dilute the Pd sites (i.e., less contiguous sites) with this effect stronger from PdP_2 than Pd_3P. The excellent performance was then related to the crystal structure with PdP_2 which is thought to form well-isolated Pd atoms which predominantly possess P as the nearest neighbors. Longer term tests with 2% PdP_2/TiO_2 suggested that stable ethylene selectivity of 82% could be obtained under competitive conditions for 50 h TOS. These results demonstrate that the addition of P to Pd catalysts offer an intriguing way to control structure and selectivity in selective hydrogenation reactions.

Acknowledgements

This work was supported by the National Key Research and Development Program of China (2016YFB0301601), National Natural Science Foundation of China.

References

[1] A. Borodziński, G. C. Bond, Catal. Rev. 48 (2006) 91-144.
[2] A. Borodziński, G. C. Bond, Catal. Rev. 50 (2008) 379-469.
[3] S. A. Nikolaev, I. L. N. Zanaveskin, V. V. Smirnov, V. A. Averyanov, K. I. Zanaveskin, Russ. Chem. Rev. 78 (2009) 231-247.
[4] A. J. McCue, J. A. Anderson, Front. Chem. Sci. Eng. 9 (2015) 142-153.
[5] C. A. Gärtner, A. van Veen and J. A. Lercher, ChemCatChem 5 (2013) 3196 –3217.
[6] J. J. Siirola, AIChE J. 60 (2014) 810-819.
[7] M. Krajčí, J. Hafner, J. Catal. 312 (2014) 232–248
[8] F. Studt, F. Abild-Pedersen, T. Bligaard, R. Z. Sørensen, C. H. Christensen, J. K. Nørskov, Science 320 (2008) 1320.
[9] M. Armbrüster, K. Kovnir, M. Friedrich, D. Teschner, G. Wowsnick, M. Hahne, P. Gille, L. Szentmiklósi, M. Feuerbacher, M. Heggen, F. Girgsdies, D. Rosenthal, R. Schlögl, Y. Grin, Nat.

Mater. 11 (2012) 690-693.
[10] N. A. Khan, S. Shaikhutdinov, H. J. Freund, Catal. Letters. 108 (2006) 159–164.
[11] W. Ludwig, A. Savara, K. H. Dostert, S. Schauermann, J. Catal. 284 (2011) 148–156.
[12] M. García-Mota, B. Bridier, J. Pérez-Ramírez, N. López, J. Catal. 273 (2010) 92–102.
[13] B. Yang, R. Burch, C. Hardacre, G. Headdock, P. Hu, J. Catal. 305 (2013) 264–276.
[14] Y. Liu, Y. He, D. Zhou, J. Feng, D. Li, Catal. Sci. Technol. 6 (2016) 3027-3037.
[15] Y. N. Liu, J. Y. Zhao, Y. F. He, J. T. Feng, T. Wu and D. Q. Li, J. Catal. 2017, 348,135-145.
[16] S. A. Nikolaev, V. V. Smirnov, Catal. Today. 147S (2009) S336–S341.
[17] G. Pei, X. Liu, A. Wang, A. F. Lee, M. A. Isaacs, L. Li, X. Pan, X. Yang, X. Wang, Z. Tai, K. Wilson, T. Zhang, ACS Catal. 5 (2015) 3717–3725.
[18] A. J. McCue, R. T. Baker, J. A. Anderson, Faraday Discuss. 18 (2016) 499-523.
[19] Y. N. Liu, J. T. Feng, Y. F. He, J. H. Sun and D. Q. Li, Catal. Sci. Technol.,2015, 5,1231
[20] G. Kyriakou, M. B. Boucher, A. D. Jewell, E. A. Lewis, T. J. Lawton, A. E. Baber, H. E. Tierney, M. Flytzani-Stephanopoulos, E. C. H. Sykes, Science 335 (2012) 1209-1212.
[21] Q. Fu, Y. Luo, ACS Catal. 3 (2013) 1245–1252.
[22] A. J. McCue, C. J. McRitchie, A. M. Shepherd, J. A. Anderson, J. Catal. 319 (2014) 127–135.
[23] A. J. McCue, A. M. Shepherd, J. A. Anderson, Catal. Sci. Technol. 5 (2015) 2880–2890.
[24] A. J. McCue, J. A. Anderson, J. Catal. 329 (2015) 538–546.
[25] A. J. McCue, A. Gibson, J. A. Anderson, Chem. Eng. J. 285 (2016) 384–391.
[26] D.L. Trimm. I. O. Liu, N. W. Cant, J. Mol. Catal. A: Chem. 307 (2009) 13−20.
[27] F. M. McKenna, J. A. Anderson, J. Catal. 281 (2011) 231-240.
[28] F. M. McKenna, L. Mantarosie, R. P. K. Wells, C. Hardacre, J. A. Anderson, Catal. Sci. Technol. 2 (2012) 632-638.
[29] A. J. McCue, F. M. McKenna, J.A. Anderson, Catal. Sci. Technol. 5 (2015) 2449-2459.
[30] D. Albani, G. Vilé, S. Mitchell, P. T. Witte, N. Almora-Barrios, N. López, J. Pérez-Ramírez, J, Catal. Sci. Technol. 6 (2016) 1621-1631.
[31] J. Osswald, K. Kovnir, M. Armbrüster, R. Giedigkeit, R.E. Jentoft, U. Wild, Y. Grin, R. Schlögl, J. Catal., 258 (2008) 219–227.
[32] M. Friedrich, S. A. Villaseca, L. Szentmiklósi, D. Teschner, M. Armbrüster, Materials, 6 (2013) 2958–2977.
[33] L. Shao, W. Zhang, M. Armbrùster, D. Teschner, F. Girgsdies, B. Zhang, O. Timpe, M. Friedrich, R. R. Schlögl, D. Sheng Su, Angew. Chem. Int. Ed. 50 (2011) 10231-10235.
[34] G. Vilé, B. Bridier, J. Wichert, J. Pérez-Ramírez, Angew. Chemie - Int. Ed. 51 (2012) 8620–8623.
[35] G. Vilé, P. Dähler, J. Vecchietti, M. Baltanás, S. Collins, M. Calatayud, A. Bonivardi, J. Pérez-Ramírez, J. Catal. 324 (2015) 69–78.
[36] D. Albani, M. Capdevila-Cortada, G. Vilé, S. Mitchell, O. Martin, N. López, Pérez-Ramírez, Angew. Chem. Int. Ed. 56 (2017) 10755-10760.
[37] G. Vilé, D. Albani, N. Nachtegaal, Z. Chen, D. Dontsova, M. Antonietti, N. López, J. Pérez-Ramírez, J., Angew. Chem. Int. Ed. 54 (2015) 11265-11269.
[38] A. J. McCue, A. Guerrero-Ruiz, I. Rodríguez-Ramos, J. A. Anderson, J. Catal. 340 (2016) 10-16.
[39] A. J. McCue, A. Guerrero-Ruiz, C. Ramirez-Barria, I. Rodríguez-Ramos, J. A. Anderson, J. Catal. 355 (2017) 40-52.

[40] B. Bachiller-Baeza, A. Iglesias-Juez, E. Castillejos-López, A. Guerrero-Ruiz, M. DiMichiel, M. Fernández-García, I. Rodríguez-Ramos, ACS Catal. 5 (2015) 5235–5241.
[41] Albani et al – submitted to Nature
[42] S. Carenco, X. F. L. Goff, J. Shi, L. Roiban, O. Ersen, C. Boissière, C. Sanchez, N. Mézailles, Chem. Mater. 23 (2011) 2270-2277.
[43] J. W. Hall, N. Membreno, J. Wu, H. Celio, R. A. Jones, K. J. Stevenson, J. Am. Chem. Soc. 134 (2012) 5532-5535.
[44] E. J. Popczun, J. R. McKone, C. G. Read, A. J. Biacchi, A. M. Wiltrout, N. S. Lewis, R. E. Schaak, J. Am. Chem. Soc. 135 (2013) 9267-9270.
[45] R. Xie, D. Battaglia and X. Peng, J. Am. Chem. Soc. 129 (2007) 15432.
[46] R. Yan, D. Gargas, P. Yang, Nat. Photonics 3 (2009) 569.
[47] D. C. S. Souza, V. Pralong, A. J. Jacobson and L. F. Nazar, Science 296 (2002) 2012-2015.
[48] J. Cabana, L. Monconduit, D. Larcher and M. R. Palacín, Adv. Mater. 22 (2010) 170-192.
[49] Y. Liang, Q. Liu, A. M. Asiri, X. Sun, Y. Luo, ACS Catal. 4 (2014) 4065-4069.
[50] Z. Xing, Q. Liu, A. M. Asiri, X. Sun, ACS Catal. 5 (2014) 145-149.
[51] A-M. Alexander, J.S.J. Hargreaves, Chem. Soc. Rev. 39 (2010) 4388-4401.
[52] S. T. Oyama, X. Wang, Y. K. Lee, W. J. Chun, J. Catal. 221 (2004) 263.
[53] J. A. Cecilia, A. Infantes-Molina, E. Rodríguez-Castellón, A. Jiménez-López, J. Catal. 263 (2009) 4.
[54] X. Wang, P. Clark, S. T. Oyama, J. Catal. 208 (2002) 321.
[55] J. A. Cecilia, A. Infantes-Molina, E. Rodríguez-Castellón, A. Jiménez-López, Appl. Catal. B: Environ. 92 (2009) 100.
[56] L. A. Rupflin, J. Mormul, M. Lejkowski, S. Titlbach, R. Papp, R. Gläser, M. Dimitrakopoulou, X. Huang, A. Trunschke, M. G. Willinger, R. Schlögl, F. Rosowski, and S. A. Schunk, ACS Catal. 7 (2017) 3584-3590.
[57] Y. D. Chen, C. M. Li, J. Y. Zhou, S. T. Zhang, D. M. Rao, S. He, M. Wei, D. G. Evans, and X. Duan, ACS Catal. 5 (2015) 5756-5765.
[58] M. Zhou Chem. Asian. J. 11 (2016) 461-464.
[59] R. H. Bowker, M. C. Smith, B. A. Carrillo, M. E. Bussell, Top Catal. 2012 (55) 999-1009.
[60] L. B. McCusker, R. B. Von Dreele, D. E. Cox, D. LoueÈr and P. Scardi, J. Appl. Cryst. 32 (1999) 36-50.
[61] M. S. Ide, B. Hao, M. Neurock, R. J. Davis, ACS Catal. 2 (2012) 671.
[62] D. Pakhare, V. Schwartz, V. Abdelsayed, D. Haynes, D. Shekhawat, J. Poston, J. Spivey, J. Catal. 316 (2014) 78.
[63] P. Weisz, C. Prater, Adv. Catal. 6 (1954) 143-196.
[64] J. Osswald, R. Giedigkeit, R. Jentoft, M. Armbrüstera, F. Girgsdiesa, K. Kovnira, T. Resslerc, Y. Grinb, R. Schlöglet, J. Catal. 258 (2008) 210-218.
[65] D. E. Mears, Industrial & Engineering Chemistry Process Design and Development 10 (1971) 541-547.
[66] S. Rundqvist, L. O. Gullman, Acta Chem. Scand. 14 (1960) 2246-2247.
[67] W. H. Zachariasen, Acta. Cryst. 16 (1963) 1253-1255.
[68] B. Yang, R. Burch, C. Hardacre, G. Headdock, P. Hu, J. Catal. 305 (2013) 264-276.
[69] J. Sá, G. D. Arteaga, R. D. Daley, J. Bernardi and J. A. Anderson, J. Phys. Chem. B 110 (2006) 17090-17095.

[70] I. Witónska, A. Królak and S. Karski, J. Mol. Catal. A: Chem. 331 (2010) 21-28.
[71] M. Boudart, H. S. Hwang, J. Catal. 39 (1975) 44-52.
[72] G. Yang, Y. Chen, Y. Zhou, Y. Tang, T. Lu, Electrochem. Commun. 12 (2010) 492–495.
[73] H. Sun, J. Xu, G.Fu, X. Mao, L. Zhang, Y. Chen, Y. Zhou, T. Lu, Y. Tang, Electrochimica Acta, 59 (2012) 279-283.
[74] S. P. Lee, Y. W. Chen, Ind. Eng. Chem. Res. 38 (1999) 2548-2556
[75] W. J. Zhou, J. Y. Lee, J. Phys. Chem. C 112 (2008) 3789.
[76] C. N. Rao, K. K. Rao, Ca. J. Phys. 42 (1964) 1336-1342.
[77] Y. Luo, S. A. Villaseca, M. Friedrich, D. Teschner, A. Knop-Gericke, M. Armbrùster, J. Catal. 338 (2016) 265-272.